PHYSICAL REVIEW B **68**, 081202(R) (2003)

Creation of supercooled exciton gas and transformation to electron-hole droplets in diamond

Masaya Nagai,[1,*] Ryo Shimano,[1,2] Kenji Horiuchi,[3] and Makoto Kuwata-Gonokami[1,2,†]
[1]*Department of Applied Physics, The University of Tokyo, and Cooperative Excitation Project ERATO, Japan Science and Technology Corporation (JST), 7-3-1, Hongo, Bunkyo-ku, Tokyo 113-8656, Japan*
[2]*Solution Oriental Research for Science and Technology (SORST), JST, 7-3-1, Hongo, Bunkyo-ku, Tokyo 113-8656, Japan*
[3]*Frontier Laboratory, R&D Planning Department, Tokyo Gas Co., Ltd. 1-7-7, Suehiro-cho, Tsurumi-ku, Yokohama 230-0045, Japan*
(Received 7 May 2003; published 12 August 2003)

We investigated the formation dynamics of electron-hole droplets in a high-purity single crystal diamond under photoexcitation near the band gap using time-resolved emission spectroscopy. Below the exciton Mott transition density, photogenerated carriers are cooled, and exciton emission appears within 30 ps. A broad emission band of droplets rises slowly, accompanied with a reduction in the exciton emission intensity in the next hundred picoseconds. This spectral change indicates the initial formation of low-temperature supersaturated exciton gas and subsequent spatial condensation of dense exciton gas into electron-hole droplets.

DOI: 10.1103/PhysRevB.68.081202 PACS number(s): 71.35.Ee, 71.30.+h, 71.35.Lk

A photoexcited electron-hole (e-h) system in semiconductors has been attracting interest for the study of many-body quantum physics in particles' system with the Coulomb interaction.[1] This is because a small effective mass of bipolar carriers and large dielectric constant in semiconductors enhance the quantum mechanical effects, which can manifest themselves in various and unique macroscopic phenomena. Another important reason is that changing the intensity and duration of the light pulses can easily control the density and temperature of the photoexcited carriers in semiconductors. Moreover, recent advances in ultrafast laser techniques have made it possible to create essentially nonequilibrium ensembles whose intrinsic dynamics can be probed by the method of ultrafast laser spectroscopy.

At low-excitation densities, an electron and hole form an electrically neutral composite particle, i.e., exciton. As soon as the average distance between excitons becomes comparable with the exciton Bohr radius a_B, i.e., at higher exciton densities, excitons become ionized due to screening of the Coulomb attraction. This transformation from the insulating exciton gas to metallic plasma is called the exciton Mott transition. At low temperature, in particular, this phase transition manifests itself as a transformation of the ensemble of quantum degenerate bosons[2] to high-density quantum degenerate fermions.[3] The exciton Mott transition is usually accompanied with a liquid-gas phase transition, which has been observed in indirect-gap semiconductors with large band degeneracy[4,5] and direct-gap polar semiconductors.[4,6,7] Being a phase transformation of the first order, this transition manifests itself as the formation of metallic e-h liquid droplet (EHD) in the exciton gas. The competition of the liquid gas and exciton Mott transitions, which gives rise to a rich variety of available phases, has been extensively studied in Ge and Si.[8,9]

Diamond has recently emerged as a good material to study the collective behavior of e-h systems.[10,11] Diamond is a wide indirect-gap semiconductor ($E_g = 5.49$ eV[12]) with a band structure similar to those of Ge and Si. Since the exciton binding energy in diamond is as large as 80 meV,[12,13] it may be possible to discriminate among various states in a wide energy scale. Figure 1(a) shows the phase diagram of an e-h system in diamond.[11] Using Thomas-Fermi screening approximation, the critical density of the exciton Mott transition is described as $n_{Mott}^{TF} = (4a_B)^{-3} = 4 \times 10^{18}\text{cm}^{-3}$. At this density, the Fermi temperatures of the electron and hole are 141 K and 71 K, respectively, and the critical temperature of the exciton Bose-Einstein condensation (BEC) is 11 K. However, the interaction between carriers leads to the instability of the quantum degenerate phases in the vicinity of the Mott density; as a result, these phases are hidden inside the phase-separated region, where the metallic liquid phase and the exciton gas phase coexist. The excitation density dependence of the time-integrated emission spectra clearly shows the occurrence of such phase separation. Figures 1(b,c) shows the time-integrated luminescence spectra of photoexcited diamond at 12 K. At low-excitation density, a narrow transverse optical (TO) phonon-assisted free-exciton line at 5.27 eV dominates the luminescence [Fig. 1(b)].[13] Above the

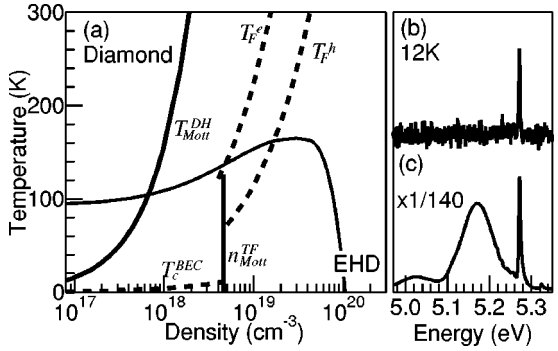

FIG. 1. (a) Phase diagram of an e-h system in diamond (Ref. 11). Two bold lines indicate the Mott criterion given by the Thomas-Fermi and the Debye-Huckel-type screening approximations. A thin curve is the boundary of the liquid-gas phase transition with a simple Guggenheim model (Ref. 16) with the parameters of $T_c = 165$ K and $n_c = 3 \times 10^{19}$ cm^{-3}. Dashed curves indicate criterion of excitonic BEC and the Fermi degenerate of electron and hole. The figures on the right show the time-integrated emission spectra in diamond at 12 K under subpicosecond pulse excitation, where the excitation densities are (b) 0.002 mJ/cm^2 and (c) 17 mJ/cm^2.

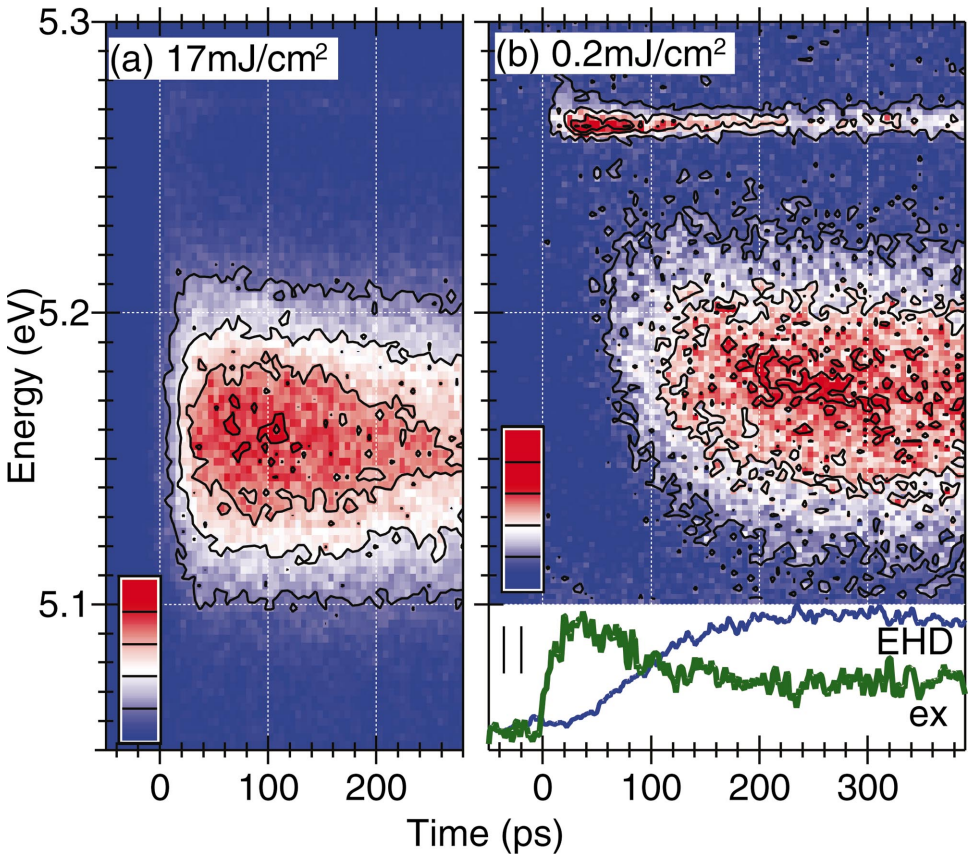

FIG. 2. (Color) Time-resolved emission spectra at 12 K. The excitation density is (a) 17 mJ/cm^2 and (b) 0.2 mJ/cm^2. Two curves in lower figure show the temporal evolution of the exciton and EHD emission intensities at the excitation density of 0.2 mJ/cm^2.

excitation density of 0.01 mJ/cm^2, a broad TO phonon-assisted EHD emission band centered at 5.15 eV appears [Fig. 1(c)].[10,14] A density in EHD of $n_0=1\times10^{20}$ cm^{-3} and a critical temperature of $T_c=165$ K are obtained from spectral line shape analysis in time-resolved emission measurements with subpicosecond pulse excitation.[10] These values are consistent with the values obtained from the temperature dependence of emission spectra under quasi-cw excitation conditions.[14,15] By substituting the experimentally obtained critical temperature and density to the Guggenheim empirical formula,[16] we can calculate the boundary of the phase-separated region that is shown in Fig. 1(a) by a thin curve. The BEC criterion is observed to sink at the very bottom of this phase coexistence area. However, our recent experimental findings indicate that the phase separation takes finite time of about several tens of picoseconds.[10] During this time, the e-h ensemble can form a quasiequilibrium metastable state. If the e-h system cools down to the lattice temperature before the spatial condensation occurs, we may have a chance to reveal the collective phenomena of the ensemble of excitons at low temperature. In this report, we measure time-resolved emission spectra in diamond at different excitation densities to reveal the mechanism of EHD formation and investigate the collective metastable e-h state, which exists in the nonequilibrium region of the phase diagram.

A single crystal diamond with the size of $2\times2\times0.5$ mm grown by the high-temperature and high-pressure method was used. The sample was mounted in a closed cycled cryostat free from any strain at the temperature of 12 K. The excitation light was the fourth harmonic of a regenerative amplified mode-locked Ti:sapphire laser set to 870 nm (0.2 ps pulse duration and 1 kHz repetition rate). Intense ultraviolet pulse was generated via the efficient sum frequency generation process in a β-BaB_2O_4 crystal with a thickness of 0.3 mm, which was irradiated by the fundamental pulse and its third harmonic. The photon energy of excitation 5.70 eV (217.5 nm) was above the indirect-gap, where the penetration depth was 15 μm.[17] The excitation pulse was focused on a sample with a spot size of 70 μm. The average carrier density could be easily controlled up to 8×10^{19} cm^{-3}. The luminescence was measured using a spectrometer with a focal length of 50 cm and a Streak camera (Hamamatsu 1955). The temporal resolution and spectral resolution were 17 ps and 0.2 nm, respectively.

Figure 2(a) shows the contour plot (the longitudinal and transverse axes show the photon energy and time, respectively) of time-resolved emission at the excitation density of 17 mJ/cm^2. Note that the corresponding time-integrated spectrum is shown in Fig. 1(c). The average e-h density, which can be estimated from the excitation photon flux and absorption coefficient, is 1.2×10^{19} cm^{-3}, i.e., it is above the exciton Mott density. Broadband EHD emission, which is shown by a red area in Fig. 2 and centered at 5.15 eV, appears right after excitation. After 20 ps, the high-energy boundary of this band (shown as the lowest-level contour of emission intensity) stays at 5.21 eV, while the low-energy boundary shifts down to 5.10 eV for 40 ps. These features indicate the spatial condensation of e-h plasma gas to dense EHD within several tens of picoseconds, reproducing the

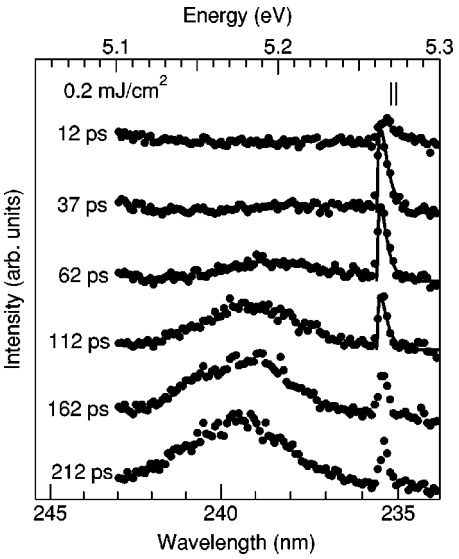

FIG. 3. Time-resolved emission spectra at an excitation density of 0.2 mJ/cm^2 at different times. Solid curves on the results at 12, 37, 62, and 112 ps show the theoretical curves of the exciton emission of 100, 45, 40, and 40 K, respectively.

features reported in Ref. 10. After 100 ps, the EHD emission band decays in the time scale of 1 ns.

Figure 2(b) shows the time-resolved emission spectra at the moderate excitation density of 0.2 mJ/cm^2. This excitation photon flux corresponds to the average exciton density of 1×10^{17} cm^{-3}, which is below the Mott density. In this emission spectrum, both broad EHD and sharp TO phonon-assisted exciton lines can be seen. The temporal evolution of these emission intensities is shown in the inset. The exciton emission intensity reaches its maximum at 30 ps after excitation. At longer time delays, the increase in the EHD emission is accompanied by a decrease of the exciton emission intensity. As soon as the EHD emission intensity reaches its maximum at 260 ps, the exciton emission decay becomes slower. These results indicate the transformation of the exciton gas into EHD in the time from 30 to 260 ps.

Figure 3 shows the time-resolved emission spectra at the excitation density of 0.2 mJ/cm^2 and various time delays. Only a TO phonon-assisted exciton emission line appears at 12 and 37 ps, and, later, an EHD emission band slowly appears. Here, we focus on the line shape of exciton emission, which is asymmetric and has a tail in the high-energy side. This tail becomes narrower with time. The exciton line shape is determined by the exciton density of states weighted by the Maxwell-Boltzmann distribution as the following:

$$n(E)=\sqrt{E}\exp(-E/k_BT_{eff}), \tag{1}$$

where E is the kinetic energy of the exciton and T_{eff} is its effective temperature. This equation allows us to obtain the effective temperature from the spectrum of exciton emission. The solid lines in Fig. 3 show the calculated emission spectra at $T_{eff}=100$ K at 12 ps, 45 K at 37 ps, and 40 K at 62 ps. Although the spectral resolution of 4 meV does not allow us to extend this analysis for longer time delays, our results indicate that photoexcited carriers are cooled rapidly towards

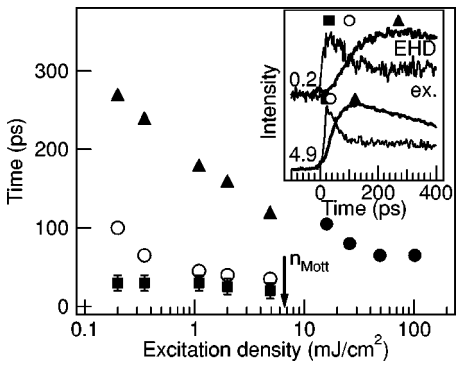

FIG. 4. The excitation density dependence of EHD formation time. Closed triangles and open circles show the time of the maximum and half-maximum EHD emission intensity, respectively. Closed circles show the formation time of EHD at the excitation density above the Mott criterion (Ref. 10). Closed squares show the time of maximum exciton emission intensity. The inset shows the temporal evolution of EHD emission (solid curves) and exciton emission (bold curves) intensities at the excitation density of 0.2 and 4.9 mJ/cm^2.

supercooled and high-density exciton gas at a few tens of Kelvins. At longer time delays, the density fluctuation of excitons results in the slow formation of EHD.

The obtained cooling time from the line shape analysis almost coincides with the time when the exciton emission reaches its maximum. This indicates that the thermalization of carriers takes place accompanied with the formation of excitons. Closed squares in Fig. 4 show the dependence of the rise time on the excitation density. The inset in Fig. 4, which shows the temporal evolution of the exciton and EHD emission intensity at the density of 0.2 and 4.9 mJ/cm^2, clarifies the definition of the rise time. It is clear that the rise time of the exciton emission does not depend on the excitation density and remains 30 ps below the Mott density. This rapid rise is caused by the efficient carrier phonon interaction via a large deformation potential[18] and high thermal conductivity that leads to the fast cooling of the lattice.[12] Since this cooling time is much shorter than the exciton lifetime ($\approx$100 ns) and EHD lifetime (1 ns),[10] the spatial phase separation occurs after dense exciton gas is cooled to the sample temperature before the annihilation of e-h pairs. Closed triangles and open circles in Fig. 4 show the time of maximum and half-maximum EHD emission intensity, respectively, below the Mott density, and closed circles show the time to transform the plasma gas into EHD above the Mott density.[10] These three times can be considered as the major characteristics of the EHD formation. In the dilute density region, the EHD formation slows down. In particular, at the excitation density of 0.2 mJ/cm^2, the EHD emission intensity reaches its maximum at 260 ps and its half-maximum at 100 ps. This indicates that the supercooled exciton gas reaches quasiequilibrium within 100 ps. Recent theoretical calculation indicates that the BEC-type correlation builds up within a few nanoseconds.[19] This supports the possibility to observe BEC-like phase by reducing the system temperature to sustain the metastable supercooled for longer period.

Finally, the temporal evolution of the EHD emission will

be discussed. In Fig. 2(b), EHD emission appears at the peak position of 5.20 eV at 50 ps. The EHD emission band shifts toward the low-energy side with an increase of its intensity with time. The emission line shape does not change after 300 ps, which coincides with the time when EHD emission intensity reaches its maximum. The lack of change in the line shape after 300 ps implies that the system has reached an equilibrium, i.e., the droplets have achieved a macroscopic size, forming a uniform e-h liquid phase. On the other hand, the strong change of the emission spectrum during the time interval from 50 to 300 ps indicates that the e-h system is far from the equilibrium liquid phase. During the nucleation and growth of EHD, the emission band is expected to dominate the emission of clusters containing several e-h pairs. Such a small carrier ensemble should have very different properties in comparison with a continuous metallic phase. A study of these properties may lead to new aspects in the crossover from the degenerate boson to degenerate fermion system. Correspondingly, further systematic measurements in the quantum degenerate regime, which can be achieved by excitation with low excess kinetic energy and low lattice temperature, are required.

In summary, the time-resolved emission spectra of photoexcited carriers in diamond were measured below the Mott density with band-to-band excitation. The transformation of quasistable and supercooled exciton gas into metallic liquid droplets was observed. The observation of the low-temperature supersaturated exciton gas can provide access to quantum degenerate phases existing in the nonequilibrium region on the phase diagram.

The authors would like to thank Yu. P. Svirko for fruitful discussions and also acknowledge A. Ishikawa and T. Ogawa for stimulating discussions. This work was supported by a Grant-in-Aid for COE Research from the Ministry of Education, Science, Sports, and Culture of Japan.

*Present address: Department of Physics, Kyoto University, Kyoto 606-8502, Japan.

†Author to whom correspondence should be addressed. Email address: gonokami@ap.t.u-tokyo.ac.jp

[1] C.F. Klingshirin, *Semiconductor Optics* (Springer, Berlin, 1997).

[2] E. Hanamura and H. Haug, Phys. Rep., Phys. Lett. **33**, 209 (1977).

[3] M. Randeria, in *Bose-Einstein Condensation*, edited by A. Griffin, D.W. Snoke, and S. Stringari (Cambridge University Press, Cambridge, 1995) p. 355.

[4] *Electron-Hole Droplets in Semiconductors*, edited by C.D. Jeffries and L.V. Keldysh (North-Holland, Amsterdam, 1983).

[5] S.G. Tikhodeev, Sov. Phys. Usp. **28**, 1 (1985).

[6] K. Bohnert *et al.*, Z. Phys. B: Condens. Matter **42**, 1 (1981).

[7] M. Nagai and M. Kuwata-Gonokami, J. Lumin. **100**, 233 (2002).

[8] A.H. Simon, S.J. Kirch, and J.P. Wolfe, Phys. Rev. B **46**, 10 098 (1992).

[9] L.M. Smith and J.P. Wolfe, Phys. Rev. B **51**, 7521 (1995).

[10] R. Shimano, M. Nagai, K. Horiuch, and M. Kuwata-Gonokami, Phys. Rev. Lett. **88**, 057404 (2002).

[11] M. Nagai, R. Shimano, K. Horiuchi, and M. Kuwata-Gonokami, Phys. Status Solidi B **238**, 509 (2003).

[12] *Properties and Growth of Diamond*, edited by G. Davies (Institution of Electrical Engineers, London, 1994).

[13] P.J. Dean, E.C. Lightowlers, and D.R. Wight, Phys. Rev. **140**, A352 (1965).

[14] K. Thonke *et al.*, Diamond Relat. Mater. **9**, 428 (2000).

[15] N. Teofilov *et al.*, Diamond Relat. Mater. **12**, 428 (2003).

[16] E.A. Guggenheim, *Thermodynamics*, 3rd ed. (North-Holland, Amsterdam, 1957), pp. 168.

[17] The penetration depth of 10 μm at 217.5 nm at room temperature is reported in Ref. 20. We determine the penetration depth at 12 K with the assumption of the same temperature dependence as that at 222 nm, where we measured 50% longer penetration depth at 10 K than that at room temperature.

[18] K. Tsukioka, Jpn. J. Appl. Phys., Part 1 **40**, 3108 (2001).

[19] O.M. Schmitt, D.B. Tram Thoai, L. Bányai, P. Gartner, and H. Haug, Phys. Rev. Lett. **86**, 3839 (2001).

[20] C.D. Clark, P.J. Dean, and P.V. Harris, Proc. R. Soc. London, Ser. A **277**, 312 (1964).